

Antimony (III) Removal from Electrolyte of Sarcheshmeh Copper Complex Refinery Using CEC370 and Purolite S957 Resins

Shahhosseini, Mehri^{*}; Saeidi, Mahboubeh^{*†}

Department of Chemistry, Faculty of Science, Vali-e-Asr University of Rafsanjan, Rafsanjan, I.R. IRAN

ABSTRACT: The major goal of electric copper refinement is to manufacture high-purity cathode copper and minimize development expenditures. Elements (Bi, As, and Sb) have an adverse impact on the consistency of the ultimate cathode. Antimony is the key element in the moving sludge formation during the electrolysis phase. Increasing the electrolysis time increases the antimony content in the electrolyte and the cathode-based antimony toxicity. This research used CEC370 and Purolite S957 resins to isolate antimony (III) from the electrolyte. To evaluate the kinetics of the mechanism in static (discrete) conditions, pseudo-first and second-order, interparticle diffusion, and Elovich models were used. The results demonstrate that the pseudo-second-order model, with the greatest correlation coefficient (for CEC370 resin $R^2=0.991$ and for Purolite S957 resin $R^2=0.997$), can better estimate the kinetics of adsorption processes for both CEC370 and Purolite S957 resins. Furthermore, the results of the control phase of the ion exchange mechanism through the intraparticle diffusion models revealed that the phase of antimony (III) ions' arrival at the adsorbent film occurred at the highest rank. This may be triggered mostly by the agitation of the solution. The slope of the rating diagram (interparticle diffusion models) of CEC370 resin suggests a smaller adsorption rate than Purolite S957 resin. The saturation phase of Purolite S957 resin was achieved upon moving around 16 liters of electrolyte over the resin, and the saturation phase of CEC370 resin was achieved after moving about 10 liters of electrolyte over the resin in the ongoing process of antimony (III) elimination from the electrolyte (comprising 286 ppm antimony).

KEYWORDS: Kinetic modeling; Antimony; Sarcheshmeh copper complex refinery; CEC370 resin, Purolite S957 resin.

INTRODUCTION

Antimony (Sb, atomic number 51) is found in Group 15 of the Periodic Table directly below arsenic and has a standard atomic weight of 121.76 g/mol. Its name is of Greek origin, “anti” plus “monos”, translating to “a metal

not found alone”. This is accurate as native antimony metal is rarely found, it is usually discovered as a sulfide mineral, the most important being stibnite, Sb_2S_3 . Antimony metal is silvery in color, has a fairly low melting point for

* To whom correspondence should be addressed.

+ E-mail: Saeidi@vru.ac.ir

● Other Address: Hydrometallurgy Department, R&D Center of Sarcheshmeh Copper Complex, Kerman, IRAN
1021-9986/2022/11/3595-3606 12/\$/6.02

a metal, 630.6 °C, is very brittle and a poor conductor of heat and electricity. Similar to arsenic, it is typically found in four oxidation states: -3, 0, +3, and +5.

Antimony is among the anodic impurities of anodic copper which accumulate inside the electrolyte in the electric refinement phase of copper processing [1]. The rise in antimony content of the electrolyte must be monitored closely during the electrical processing phase to avoid pollution of the copper cathode. As its content exceeds 500 ppm, antimony sediments at the cathode decreases the efficiency of the cathode copper. The development of moving sludge and cathode fragility are often correlated with antimony processing [2-4]. The process of ion adsorption is useful for antimony elimination and has been applied in the presence of selective adsorption of biological compounds, inorganic oxide, activated carbon, and ion exchange resins [5]. Significant attention has been paid to the application of resins of ion exchange because of their greater diversity, functionality in a broad range of pH and temperature, feasibility and reconstruction. However, their usage is cost-effective at high absorption rates [6-10]. Antimony and any impurity in the copper electrolyte are typically eliminated using aminophosphonic resins often recognized as aminomethylphosphonic resins. The aminophosphonic resin has the basic form $R-\text{CH}_2\text{NHCH}_2\text{PO}_3\text{H}_2$, in which R is a phenolic or divinylbenzene polystyrene polymer [11, 14].

The aim of this research is to investigate the mechanism of antimony (III) removal from the electrolyte of Sarcheshmeh copper complex refinery using CEC370 and Purolite S957 resins.

EXPERIMENTAL SECTION

Materials and methods

The solution is a 286 ppm antimony electrolyte manufactured by the Sarcheshmeh Copper Complex Refinery. Chemical content and S957 resin were purchased from the Purolite Business; Shanghai Zhaoyu; China. Both resins had chelating effects due to their sulfonate functional groups. The resin properties, including their surface characteristics, morphology, composition, scale, organization, and porosity were evaluated by the US and SE detector surface imagery using FEI SEM QUANTA 200 electron microscopes. Elemental analysis was carried out by EDS EDAX Silicon Drift 2017 device; USA. The antimony content of the solutions was measured by flame

atomic absorption spectroscopy using the Agilent 200 series analyzer.

Test method

The tests were carried out in a discrete environment using 150 mL Erlenmeyer flasks comprising 0.1 g adsorbent and 50 mL electrolyte solution. For proper performance, the resins must be formulated and submerged throughout distilled water over 24 hours until usage. For kinetic studies, the analysis of process improvements was conducted in terms of adsorption/period at the presence of an electrolyte, utilizing antimony at a density of 286 mg / l (ppm) at 298 °K, varying sampling times up to 2 hours, and corrosion situations with 180 rpm. Adsorption kinetics is used to assess the adsorption capacity, including the surface adsorption, chemical process form, and propagation pathways. The residence period required to complete the adsorption process, as well as the instrument measure for adsorption procedures, can be calculated by studying adsorption kinetics and estimation of dissolved adsorption. One of the adsorption mechanisms is the ion exchange phase. Adsorption kinetics is defined as the study of the aspects and phases of a reaction, such as the process and the rate at which it reaches its destination. Time is regarded as a parameter in kinetics, and its concentration or associated features are regarded as functions [15]. The concentration-dependent variable can be determined using a range of methodologies. Numerous kinetic models, namely first- and second-order models, Elovich formulas, and interparticle diffusion were used for this purpose (Equations 1 to 4):

Pseudo – first – order equation :

$$\log(q_e - q_t) = \log q_e - \frac{K_1}{2.303}t \quad (1)$$

Pseudo – second – order equation:

$$\frac{t}{q_t} = \frac{1}{K_2 q_e^2} + \frac{1}{q_e} t \quad (2)$$

$$\text{Elovich equation : } q_t = \frac{1}{\beta} \ln(\alpha\beta) + \frac{1}{\beta} \ln t \quad (3)$$

$$\text{Intra – particle diffusion equation : } q_t = K_i t^{0.5} \quad (4)$$

Where q_e denotes the sum of adsorption per adsorbent component at equilibrium, q_t is the sum of adsorption per adsorbent component at any moment, t shows the time, K_1 and K are rate, and quadratic kinetic constants, respectively. α represents the constant of initial adsorption

Table 1: Kinetic parameters of antimony (III) adsorption on CEC370 and Purolite S957 resins.

CEC370	S957	Constants	Model
127	142	q_e (mg/g)	Experimental
94.623	85.31	q_e (mg/g)	Pseudo first-order
0.039	0.032	K_1 (h ⁻¹)	
0.972	0.924	R^2	Pseudo second-order
0.0005	0.0006	K_2 (mg/g.h)	
142.85	166.66	q_e (mg/g)	Elovich
0.991	0.997	R^2	
0.036	0.033	B (g/mg)	Intraparticle diffusion
32.22	45.45	α (mg/g.h)	
0.975	0.985	R^2	Intraparticle diffusion
15.98	18.54	K_i (mg/g.h ^{0.5})	
0.775	0.644	R^2	

frequency. β shows the surface coverage region and activation energy per chemical adsorption and K_i is the constant of interparticle diffusion rate [16].

A glass column with a diameter of 20.8 mm was designed to carry out sustained (columnar) examinations to eliminate antimony (III) from the refinery electrolyte. In the load column, 50 mL of the target resin in the enlarged moist form was transferred onto the resin bed with an electrolyte solution at a particular flow rate of 200 mL/h corresponding to 4BV/h.

RESULTS AND DISCUSSION

Process kinetics evaluations

Tables 1 and Figs. 1 and 2 display the effects and variables determined from process kinetics. The pseudo-quadratic adsorption kinetics provides the optimal match based on the correlation coefficients (R^2) for both CEC370 and Purolite S957 resins. The adsorption mechanism in both CEC370 and Purolite S957 resins well fitted with the pseudo-quadratic kinetic adsorption, implying that the process rate is controlled by chemical adsorption, which involves van der Waals forces attributable to electron sharing or exchange between the adsorbed molecules and the resin functional groups. A framework for intraparticle diffusion described the process and level of control or limitation of the ion exchange phase and the number of adsorption stages.

Figs. 3 and 4 demonstrate the adsorption rate of antimony (III) ions for both resins; the pace is determinable by the slope of each section [17]. The lower slope of the CEC370 resin graph showed that the resin's adsorption intensity was smaller than that of the Purolite S957 Resin. According to this model, ion adsorption was achieved in three phases. The first step involved the movement of ions from the solution to the liquid layer, the second phase was the movement of the ions from the film to the absorber layer while the third one involved their transmission from the surface to the internal regions of the resin. Naturally, phases two and three are often combined, i.e. absorption occurs in two phases [18]. Correlation of the slope of each stage revealed that the first phase (transition of antimony (III) ions to the adsorbent film in both resins) was achieved at the highest amount, even though the solution was predominantly stirred through this process.

Columnar antimony (III) elimination tests by Purolite S957 and CEC370 resins

In single-column experiments, the mechanism of adsorption of ion exchange resins was such that with the movement of the charged solution, i.e. electrolyte, the content of the targeted ion, i.e. antimony, at the column production was small. This behavior proceeded until the breakthrough point. Following the breakthrough point, the amount of antimony in the output steadily elevated, and

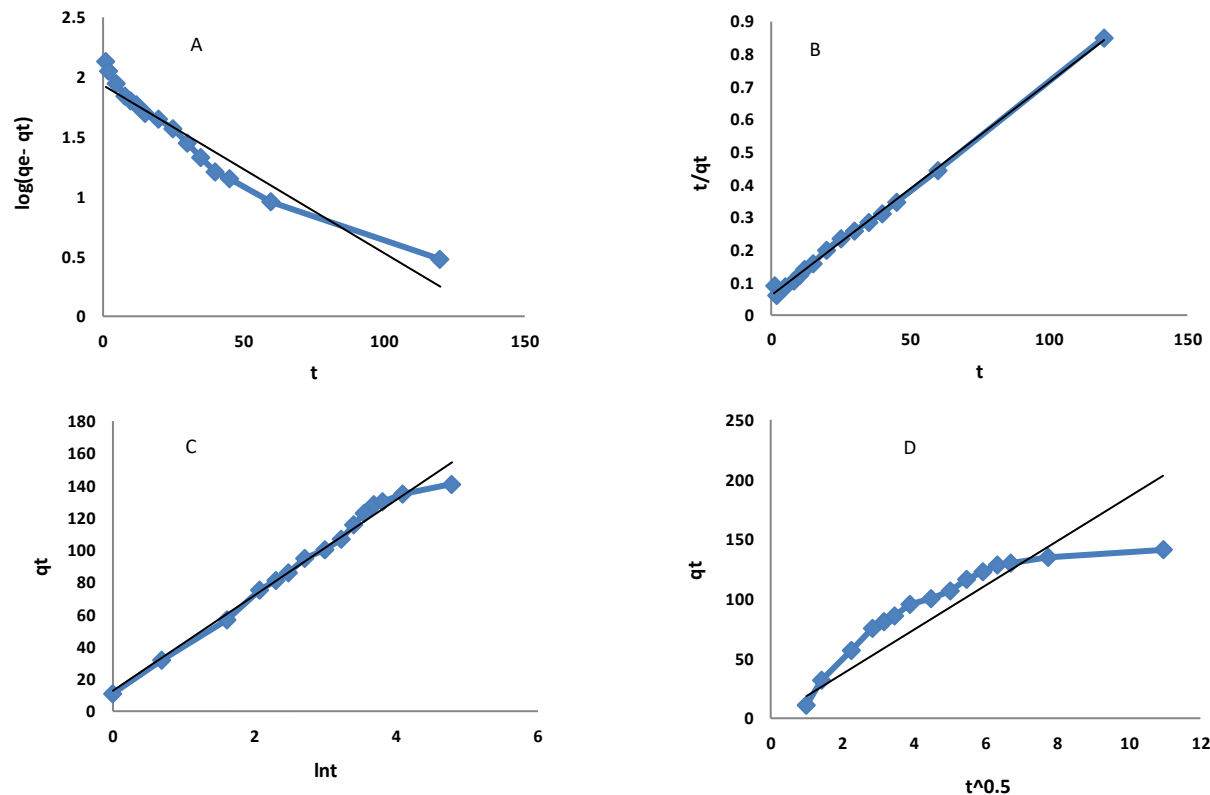


Fig. 1: Adsorption kinetics for s957 resin a) pseudo-first-order, b) pseudo-second-order, c) Elovich, and d) intraparticle diffusion models.

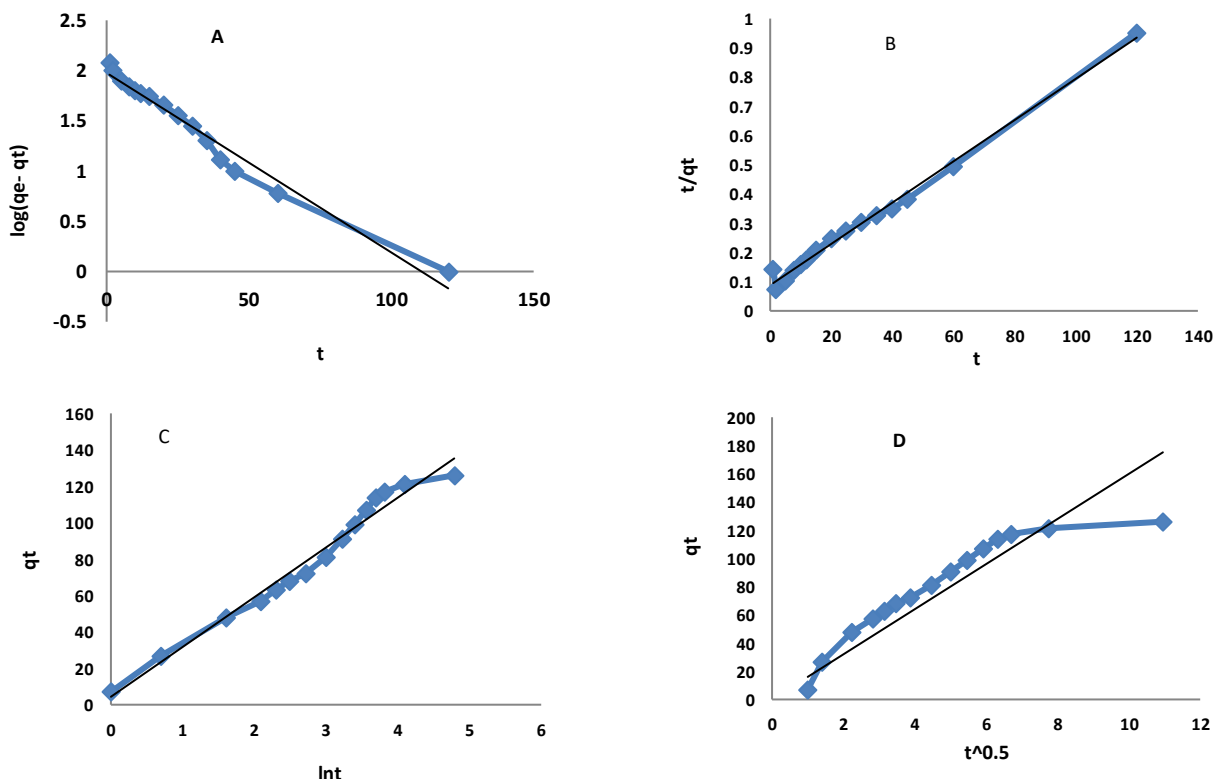


Fig. 2: Adsorption kinetics for CEC370 resin a) pseudo-first-order, b) pseudo-second-order, c) Elovich, and d) intraparticle diffusion models.

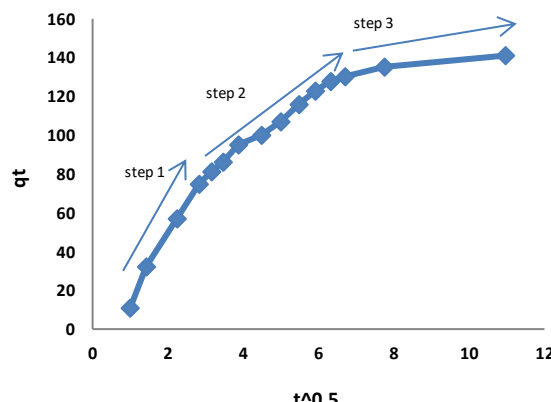


Fig. 3: Intraparticle diffusion model for s957 resin.

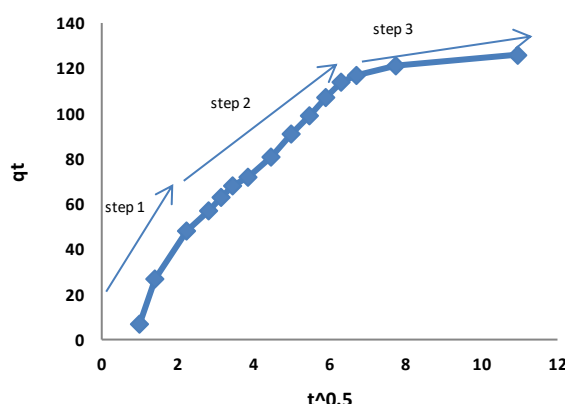


Fig. 4: Intraparticle diffusion model for CEC370 resin.

this step was maintained until the concentration of antimony input and output throughout the column was balanced (i.e. achieving the columnar saturation point). Fig. 5 indicates that the elimination of antimony (III) using Purolite S957 resin began with a 90% performance (from the beginning of the cycle to the breakthrough point). Nevertheless, when more electrolyte was passed over the resin, the antimony (III) elimination performance reduces until the resin approached saturation after around 16 liters of electrolyte (BV 324) was passed over.

At first, antimony (III) elimination from CEC370 resin occurred at high productivity according to Fig. 6. Nevertheless, owing to the structure of the single-column examination, when more electrolyte was transferred over the resin, the antimony (III) elimination performance declined until the resin saturation point was achieved when around 10 liters of electrolyte (BV 209) was transferred over the resin.

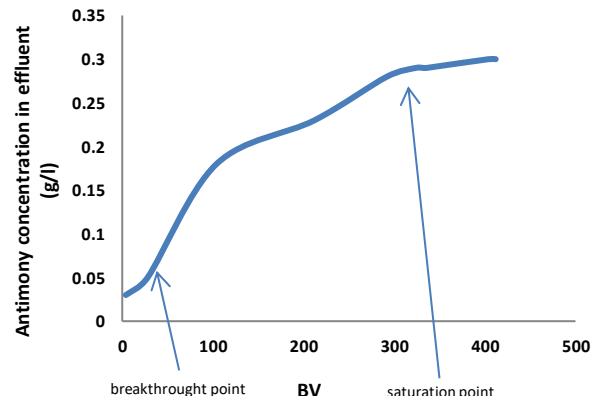


Fig. 5: Antimony (III) elimination from refinery electrolyte by Purolite S957 resin.

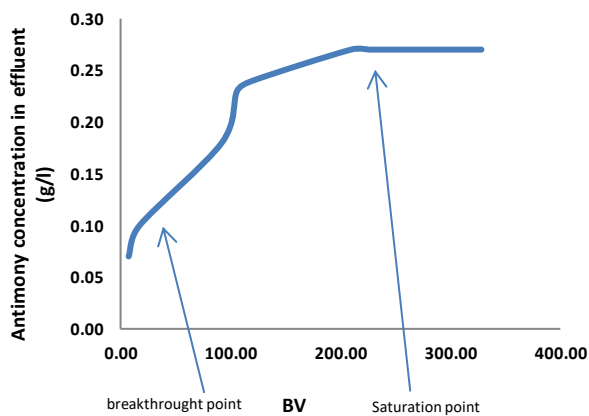


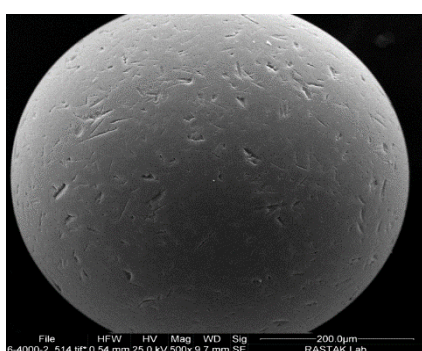
Fig. 5: Antimony (III) elimination from the refinery electrolyte by 370CEC resin.

Morphological evaluation of Purolite S957 and CEC370 resin gel particles in distilled water using Scanning Electron Microscopy (SEM) and elemental analysis (EDS)

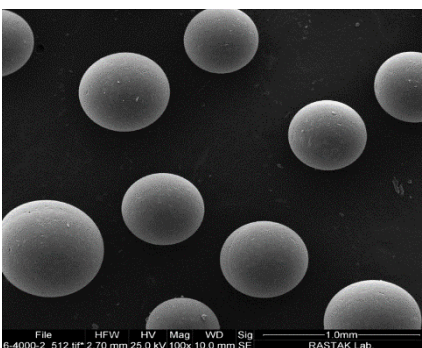
Purolite S957 and CEC370 resin were independently soaked in distilled water. Polystyrene, divinylbenzene, sulfonic acid, and phosphonic acid were present in the sample to be examined.

Figs. 7 and 8 demonstrate that the gel particles retain their spherical form. The spherical particle diameter of the gel ranged between 0.5 and 1 mm for Purolite S957 resin and 1 and 1.5 mm for CEC370 resin. Higher magnification photographs displayed an irregular surface free from porosity with little material deposition on the surface. The micron-scale surface roughness of the resin indicated its high specific surface area.

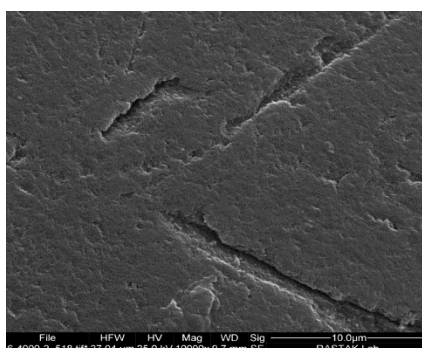
The elemental EDS analysis results are indicated in Figs. 9 and 10.



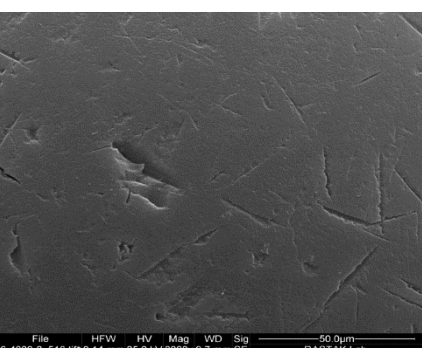
SE-SEM image at 500x magnification



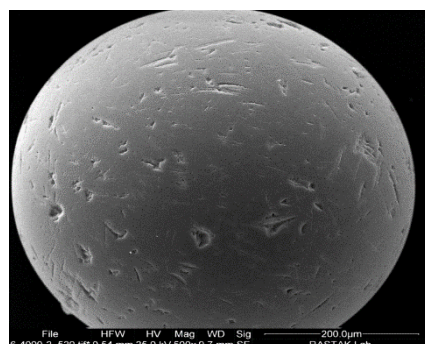
SE-SEM image at 100x magnification



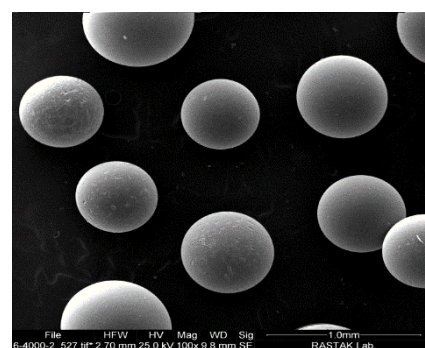
SE-SEM image at 10000x magnification



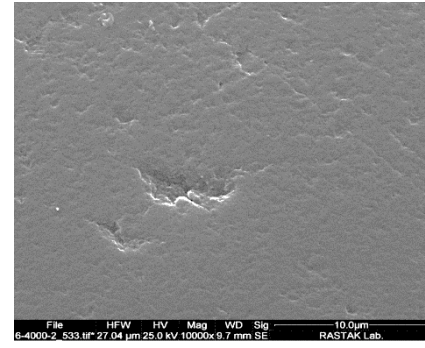
SE-SEM image at 2000x magnification



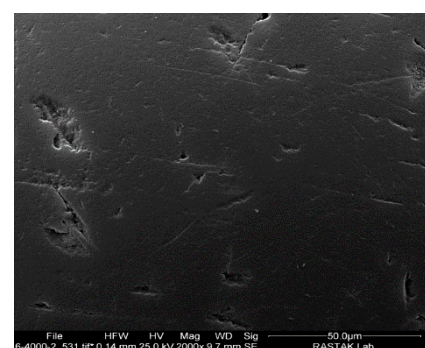
SE-SEM image at 500x magnification



SE-SEM image at 100x magnification



SE-SEM image at 10000x magnification



SE-SEM image at 2000x magnification

Fig. 7: SE-SEM image of Purolite S957 resin.**Fig. 8: SE-SEM image of 370CEC resin.**

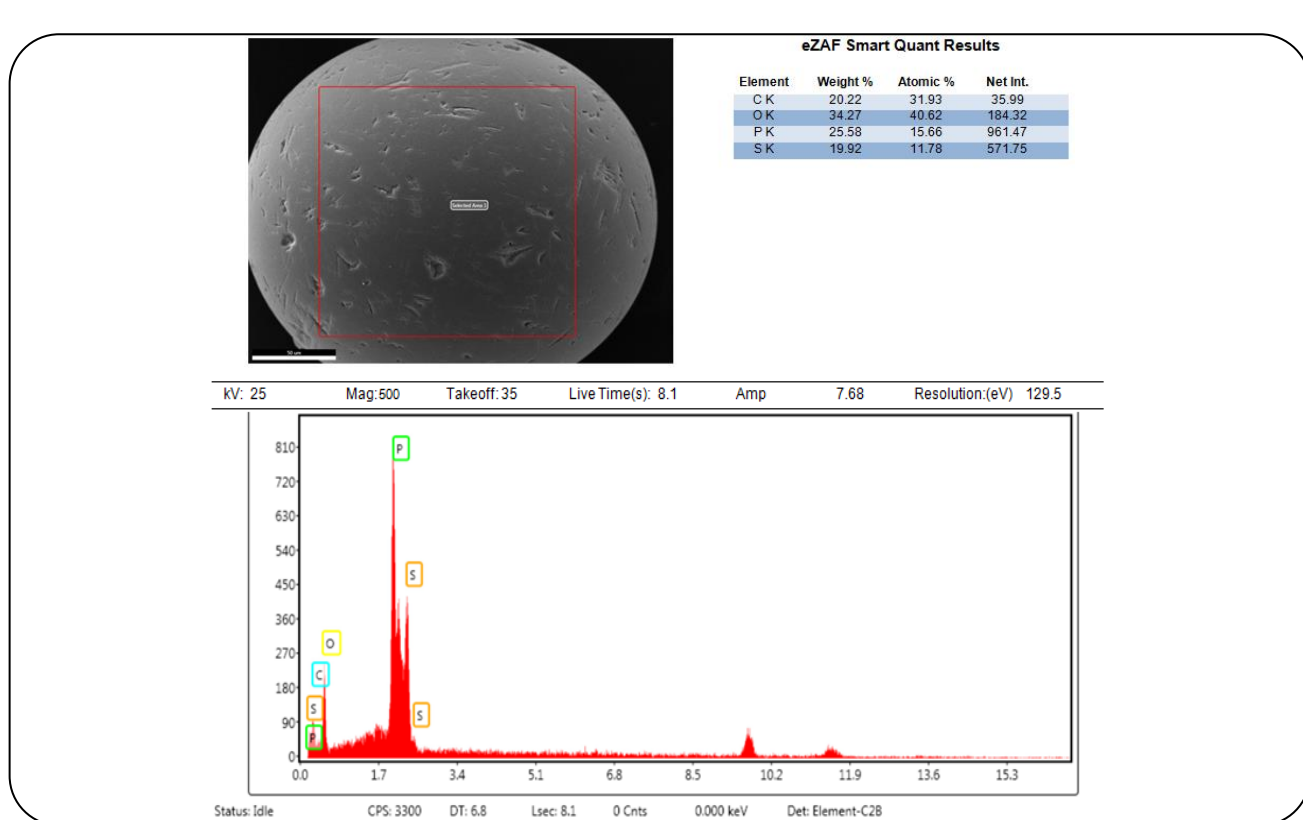
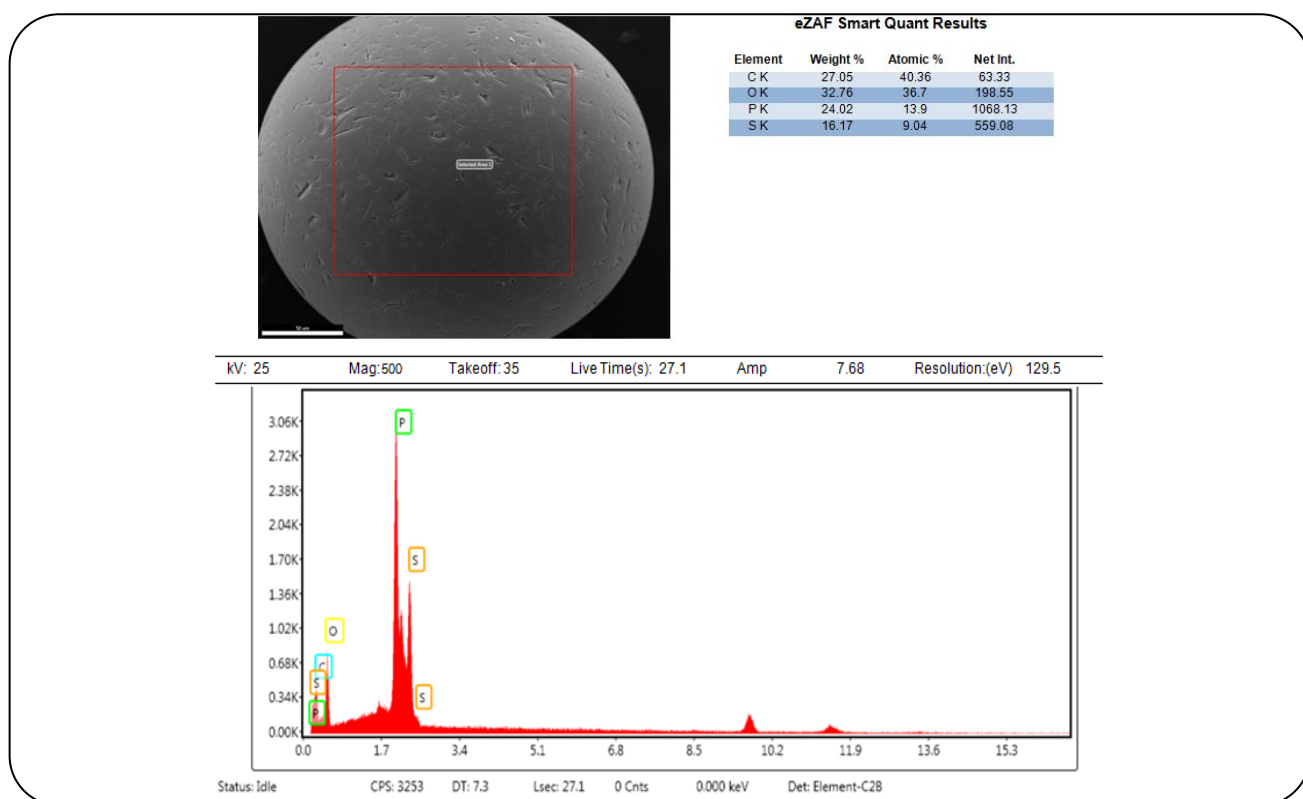
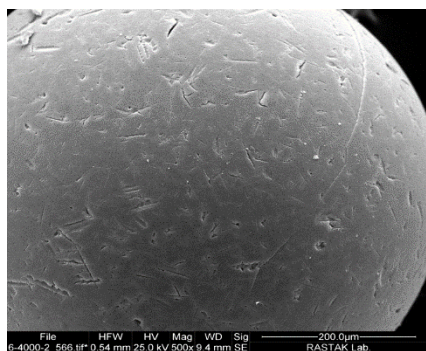
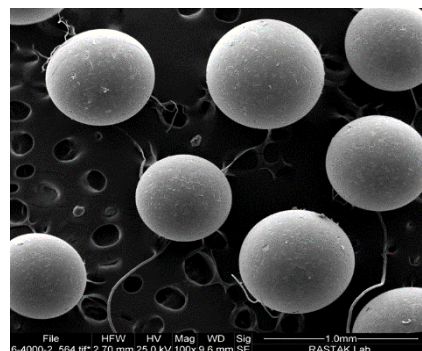


Table 2. EDS results of Purolite S957 and CEC370 resins exposed to distilled water

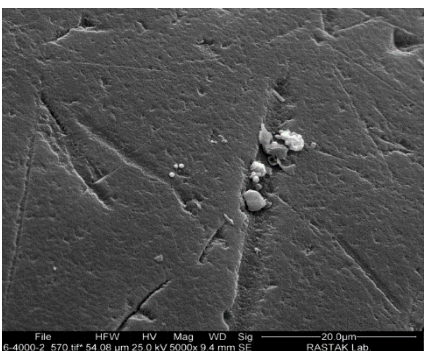
Element	Purolite S957 resin		CEC370 resin	
	Amount (wt.%)	Amount (wt.%)	Amount (wt.%)	Amount (wt.%)
Carbon	28.7	27.1	20.2	20.0
Oxygen	34.9	32.8	27.3	32.5
Phosphorus	19.3	24.2	25.6	27.1
Sulfur	17.1	16.1	19.9	20.4



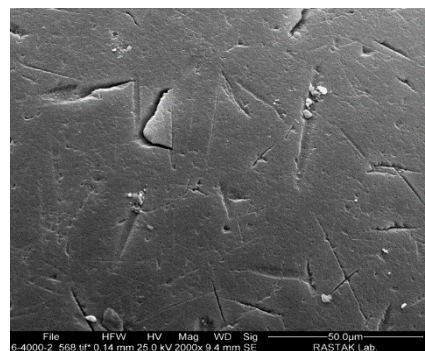
SE-SEM image at 500x magnification



SE-SEM image at 100x magnification



SE-SEM image at 10000x magnification



SE-SEM image at 2000x magnification

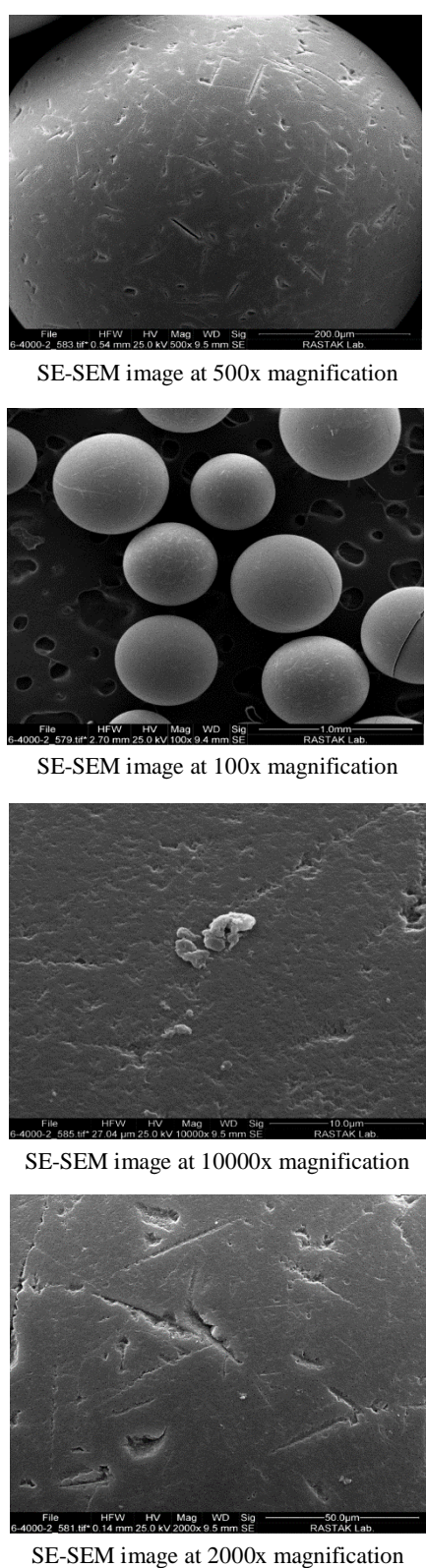
Fig. 11: SE-SEM image of Purolite S957 resin.

The EDS results confirmed the presence of hydrocarbons, phosphorus, and sulfur in the resin. Comparing the results in both regions revealed a disparity in the components of two tested spherical particles as listed in Table 2.

The majority of modifications were identified in the sum of the phosphorous element in Purolite S957 resin. Such modifications in the amount of oxygen element, however, were noted as significant in 370 CEC resin.

Evaluation of particle morphology of Purolite S957 resin gel and CEC370 resin exposed to the electrolyte of Sarcheshmeh Copper Complex Refinery using Scanning Electron Microscopy (SEM), elemental analysis (EDS), and elemental distribution map (X-Ray Map)

Purolite S957 resin and CEC370 resin were separately mixed with the electrolyte of the Sarcheshmeh Copper Refinery. This specimen contained polystyrene, divinylbenzene, sulfonic acid, phosphonic acid, bismuth, iron, nickel, arsenic, chlorine, copper, and antimony. Figs. 11 and 12

**Fig. 12: SE-SEM image of CEC370 resin.**

reveal that the spherical form of the gel particles was preserved. Higher magnification photos showed the stable nature of the spherical particles of Purolite S957 and CEC370 resins in contact with the electrolyte. Moreover, no porosity and phase aggregation were detected on the surface of resin particles.

The EDS elemental results are presented in Figs. 13 and 14.

The EDS results of Purolite S957 and CEC370 resins in contact with the electrolyte of the Sarcheshmeh Copper Refinery indicated the proper adsorption of antimony (III) ion by the spherical particles of Purolite S957 and CEC370 resin. Furthermore, the antimony (III) adsorption of Purolite S957 was higher than CEC 370. Comparing the two resins showed a little disparity in the element adsorption of the spherical particles. The adsorption efficiency of Purolite S957 and CEC370 resin in the electrolyte was nearly homogeneous. Table 3 presents a comparison of the outcomes of these evaluations.

An X-ray distribution map was used to determine the homogeneity of the particulate structure. The element chart displays each element's position with a particular color.

The X-ray map indicated the efficient and homogenous adsorption of antimony on the spherical particles of Purolite S957 and CEC370.

CONCLUSIONS

Assessment of antimony (III) ions adsorption on CEC370 resin in discrete and persistent systems led to the following conclusions:

- Based on the correlation coefficients of the models (R^2), pseudo-second-order adsorption kinetics showed a better fit for both CEC370 and Purolite S957 resins.
- According to the interparticle diffusion model, the ion adsorption mechanism on the adsorbent occurred in three phases: the transition of ions from the mixture to the liquid layer surrounding the adsorbent; the transfer of ions from the film to the adsorbent layer, and their infiltration from the surface to the internal locations of the resin.
- The lower slope of the rate diagram (interparticle diffusion models) of CEC370 resin suggests is smaller adsorption rate compared to Purolite S957 resin.
- During the columnar evaluations of antimony (III) elimination (containing 286 ppm antimony), the saturation point of Purolite S957 resin occurred after the passing

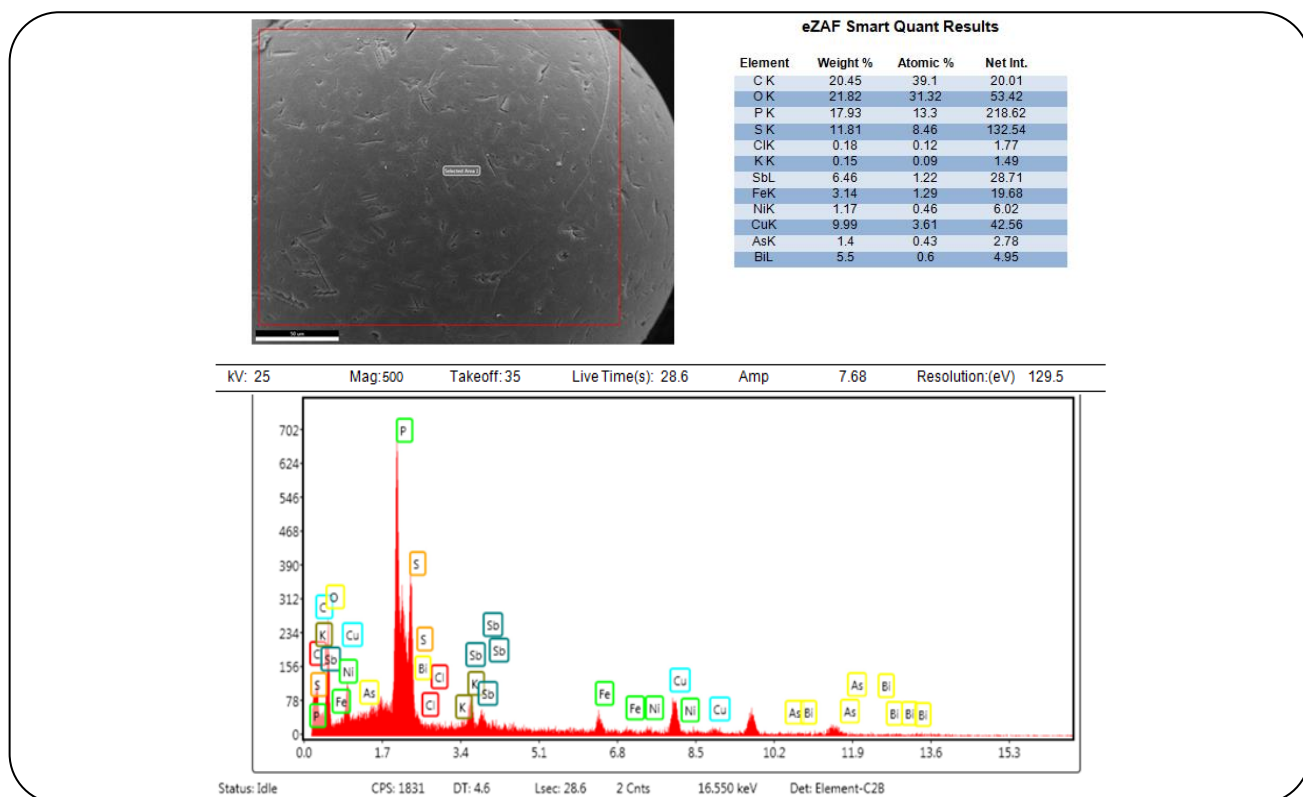
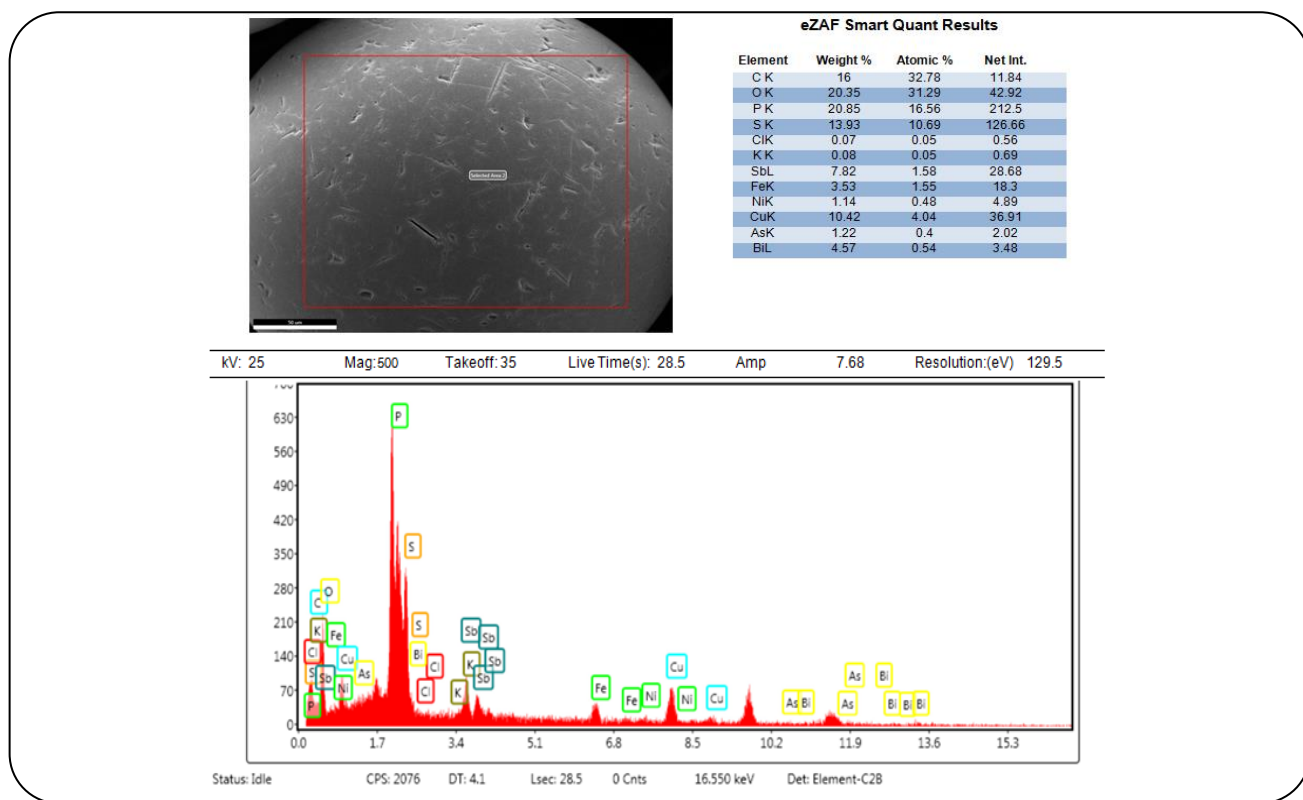
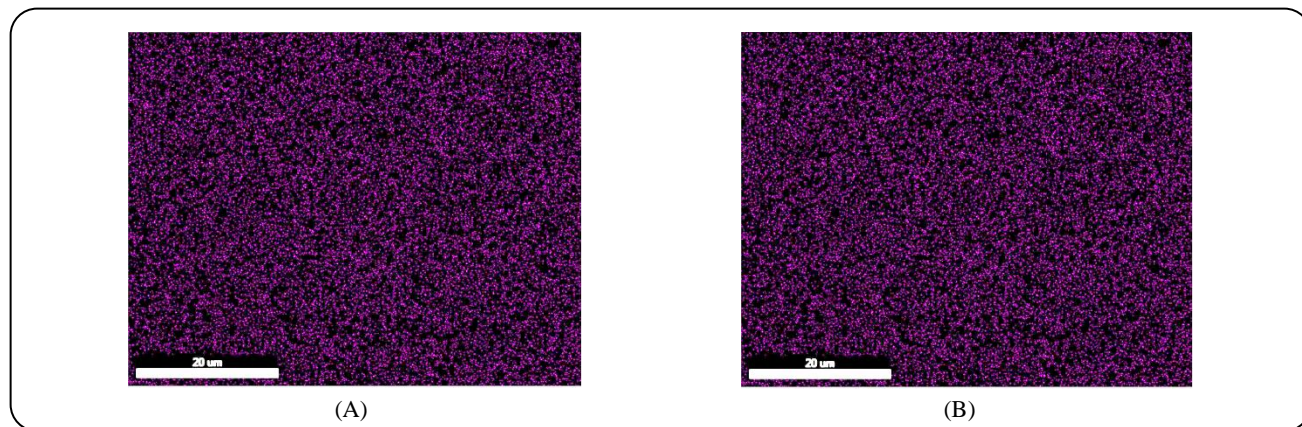
**Fig. 13:** EDS results of Purolite S957 resin exposed to the electrolyte.**Fig. 14:** EDS results of CEC370 resin exposed to the electrolyte.

Table 3: EDS results of Purolite S957 and CEC370 resins exposed to the electrolyte.

Element	Purolite S957 resin		CEC370 resin	
	Amount (wt.%)	Amount (wt.%)	Amount (wt.%)	Amount (wt.%)
Carbon	20.3	20.6	16	16.5
Oxygen	21.9	20.9	20.3	18.5
Phosphorus	17.8	19.9	20.9	20.9
Sulfur	11.8	13.1	13.9	14.4
Potassium	0.1	0	0.1	0.1
Antimony	6.5	7.3	7.8	7.5
Chlorine	0.2	0.1	0.1	0.1
Iron	3.1	3.0	3.5	3.8
Nickel	1.2	0.9	1.1	1.3
Copper	3.6	3.7	10.4	10.8
Arsenic	0.4	0.4	4.6	4.8
Bismuth	0.6	2.5	4.6	4.8

**Fig. 15: X-ray map for the antimony adsorbed on a) Purolite S957 resin, b) CEC370 resin.**

of 16 liters of electrolyte (BV 324) while CEC370 resin was saturated after passing 10 liters of electrolyte (BV 209) over the resin.

- Morphological analysis of Purolite S957 and CEC370 resin gel particles within distilled water using Scanning Electron Microscopy (SEM) revealed that the diameter of the spherical gel particles for Purolite S957 and CEC370 resins ranged in 0.5-1 mm and 1-1.5 mm, respectively. Higher magnification photos showed a smooth surface free of porosity with no material deposition on the layer. The micron-scale surface roughness indicated the large specific surface area of the samples.

- Morphological analysis of Purolite S957 and CEC370 resin gel particles exposed to the electrolyte of

the Sarcheshmeh Copper Refinery demonstrates the stability of spherical particles of Purolite S957 resin and CEC370 resin. They also indicated little porosity and small aggregation on the resin layer.

- The EDS results of Purolite S957 and CEC370 resins in contact with the electrolyte of the Sarcheshmeh Copper Refinery also revealed the higher antimony (III) adsorption capacity of Purolite S957 resin compared to CEC 370 resin. The adsorption efficiency of Purolite S957 and CEC370 in the electrolyte was nearly homogeneous.

Received: Jul. 25, 2021 ; Accepted: Dec. 20, 2021

REFERENCES

- [1] Navarro P., Alguacile F.J., Adsorption of Antimony and Arsenic from a Copper Electrorefining Solution onto Activated Carbon, *Hydrometallurgy*, **66**: 101–105 (2002).
- [2] Davis J.R. “Copper and Copper Alloys”. New York: ASM International, 3–9 (2001).
- [3] Schlesinger M., Paunovic M. “Modern Electroplating”, 5th ed. New York: Wiley, 1–6 (2011).
- [4] Salari K., Hashemian S., Baei M.T., Sb(V) removal from Copper Electrorefining Electrolyte: Comparative Study by Different Sorbents, *Transactions of Nonferrous Metals Society of China*, **27**: 440–449 (2017).
- [5] Fan H.T., Sun W., Jiang B., Wang Q.J., Li D.W., Huang C.C., Wang K.J., Zhang Z.G., Li W.X., Adsorption of Antimony(III) from Aqueous Solution by Mercapto-Functionalized Silica-Supported Organic-Inorganic Hybrid Sorbent: Mechanism Insights, *Chemical Engineering Journal*, **286**: 128–138 (2016).
- [6] Rabiul Awual M.D., Rahman I.M.M., Yaita Tkhaledque Abdul M.D., Ferdows M., pH-dependent Cu (II) and Pd (II) Ions Detection and Removal from Aqueous Media by an Efficient Mesoporous Adsorbent, *Chemical Engineering Journal*, **236**: 100–109 (2014).
- [7] Rabiul Awual M.D., Hasan Manjur M.D., Shaha A.A., Naushad U., Shiwaku H., Yaita T., Investigation of Ligand Immobilized Nano-Composite Adsorbent for Efficient Cerium(III) Detection and Recovery, *Chemical Engineering Journal*, **265**: 210–218 (2015).
- [8] Rabiul Awual M.D., Ismael M., Yaita T., El Saftys A., Shiwaku H., Okamoto Y., Suzuki S., Trace Copper(II) Ions Detection and Removal from Water Using Novel Ligand Modified Composite Adsorbent, *Chemical Engineering Journal*, **222**: 67–76 (2013).
- [9] Rabiul Awual M.D., Ring size-Dependent Crown Ether-Based Mesoporous Adsorbent for High Cesium Adsorption from Wastewater, *Chemical Engineering Journal*, **303**: 539–546 (2016).
- [10] Rabiul Awual M.D., Suzuki S., Taguchi Tshiwaku H., Okamoto Y., Yaita T., Radioactive Cesium Removal From Nuclear Wastewater By Novel Inorganic and Conjugate Adsorbents, *Chemical Engineering Journal*, **242**: 127–135 (2014).
- [11] Chiariza R., Horwitz E.P., Alexandratos S.D.. Diphenix® Resin: A Review of its Properties and Applications, *Separation Science and Technology*, **32**: 1–35 (1997).
- [12] Arexandrator S., Shelley C.A., Horwitz E.P., Chiarizia R., Bi-Functional Phenyl Monophosphonic Sulfonic Acid Ion Exchange Resin and Process for Using the Same Method, USA Patent, US 6488859 B2. (2003).
- [13] NEBEKER N, HISKEY J B. Recovery of rhenium from the copper leach solution by ion exchange, *Hydrometallurgy*, **125–126**: 64–68 (2012).
- [14] CHEN Y., HE Y., YE W., JIA L., Competitive Adsorption Characteristics of Na(I)/Cr(III) and Cu(II)/Cr(III) on GMZ Bentonite in their Binary Solution. *Journal of Industrial and Engineering Chemistry*, **26**: 335–339 (2014).
- [15] Khan M.D.A., Akhtar A., Nabi S.A., Kinetics and Thermodynamics of Alkaline Earth and Heavy Metal Ion Exchange Under Particle Diffusion Controlled Phenomenon Using Polyaniline-Sn (iv) Iodophosphate Nanocomposite, *Journal of Chemical & Engineering Data*, **59(8)**: 2677–268 (2014).
- [16] Lou Z., Zhao Z., Li Y., Shan W., Xiong Y., Fang D., Yue S., Zang S., Contribution of Tertiary Amino Groups to Re (VII) Biosorption on Modified Corn Stalk: Competitiveness and Regularity, *Bioresource Technology*, **133**: 546–554 (2013).
- [17] Wu F.-C., Tseng R.-L., Juang R.-S., Initial behavior of Intraparticle Diffusion Model Used in the Description of Adsorption Kinetics, *Chemical Engineering Journal*, **153(1-3)**: 1–8 (2009).
- [18] Igwe J., Abia A., A Bioseparation Process for Removing Heavy Metals from Waste Water Using Biosorbents, *African Journal of Biotechnology*, **5(11)**: (2006).